Molecular-dynamic simulation on the equilibrium and dynamical properties of fluids in a nano-channel

H. Hoang*, S. Kang* and Y. K. Suh*

* Department of Mechanical Engineering, Dong A University, 840 Handan-Dong, Saha-gu, Busan 604-714, Korea
(Tel : +82-051-200-6999; E-mail: haicom_quanhau@yahoo.com)

Abstract: The equilibrium molecular-dynamic simulations have been performed to estimate the properties of the three kinds of fluids (the Lennard-Jones fluid, water and aqueous sodium-chloride solution) confined between two plates that are separated by 1.086 nm; included in the equilibrium properties are the density distribution and the static structure, and the diffusivity in the dynamic property. Three kinds of fluids considered in this study are. The water molecules are modeled by using the SPC/E model and the ions by the charged Lennard-Jones particle model. To treat the water molecules, we combined the quaternion coordinates with Euler angles. We also proposed a plausible algorithm to assign the initial position and direction of molecules. The influence of polarization of water molecules as well as the presence of ions in the solution on the properties will be addressed in this study. In addition, we performed the non-equilibrium molecular-dynamic simulation to compute the flow velocity for the case with the gravitational force acting on molecules.

Keywords: Molecular-dynamic simulation, Aqueous sodium-chloride solution, Water, Lennard-Jones fluid, Nano-channel

1. INTRODUCTION

In recent years, the properties of fluid confined between two plates that are separated by a distance in the range from a few times the diameter of molecules to several nanometers have been studied by using molecular-dynamic (MD hereafter) simulation [1-5]. The characteristics of interaction among fluid molecules themselves and that between fluid and wall molecules as well as the gap between plates strongly affect the structure of fluid, i.e. the local variation of fluid properties, such as the density distribution and the radial distribution function, etc. (However, one exceptional case is for the hydrophobic walls; by using various models for the fluid-wall interaction, Kumar et al. [4] found that the properties of liquid were weakly dependent on the details of confining potential (potential between the wall and the fluid molecules) for the specific case of smooth walls). The effect of the channel gap on these properties was also investigated for both the Lennard-Jones fluid and electrolyte [1-2, 6]. With the gap of 1-4 times the diameter of molecules, the fluid showed some anomalous properties such as the equilibrium freezing temperature, solidification, static structure, etc. [4-5]. These properties are different from those of the bulk. Increasing the gap to several nanometers, however, results in the similar properties between the two [2, 6-8].

In both MD and Monte Carlo methods, the interaction among the water molecules themselves and that between water and other kinds of molecules are characterized by two kinds of forces. They are the Lennard-Jones force and the electrical force. We may well postulate that both forces are equally important in determining the equilibrium and dynamical properties of fluids. However, there are a few studies in which they only considered the Lennard-Jones force and obtained reasonable results such as the density distribution and the velocity profile [9, 10]. This implies that there are some properties of fluid confined within the channel that are weakly influenced by the electrical force.

In previous studies, in order to implement the rigid models such as SPC/E for water molecules, various algorithms like SETTLE, SHAKE and LINCS have been popularly used in MD simulation; these algorithms have also been modified to perform the energy minimization [6-8]. On the other hand, the Euler angle has been utilized to constraint the structure of water molecules [20]. This method is easier for application than the previous algorithms, i.e. SETTLE, SHAKE and LINCS, etc. However, this method has never been applied in MD simulation even though it was successfully used in the Monte Carlo simulation [11]. The reason for this may be due to difficulty in setting up the initial configuration of molecules including positions and Euler angles in such way that it produces small net force and moment of molecules.

Our main purpose in the present paper is to apply MD simulation and investigate the effect of the electrical force and presence of ions in solution on the properties of fluid in a nano-channel for three kinds of fluids. In addition, we propose that the Euler angles combined with quaternion coordinates can be used effectively to constraint the rigid structure of the water molecules. A plausible algorithm is also developed to reasonably perform the initial configuration of all the molecules. In addition, the non-equilibrium MD simulations were performed to estimate the dependence of the flow rate on the pressure gradient as well as the velocity profile across the channel.

2. MOLECULAR-DYNAMIC SIMULATION

A. Physical model

In our study, we treated three kinds of fluids. The first one is the so called Lennard-Jones fluid, in which no electric forces are considered and the coefficients ε and σ for the Lennard-Jones potential

$$u(r) = 4\varepsilon\left[\left(\frac{\sigma}{r}\right)^{12} - \left(\frac{\sigma}{r}\right)^{6}\right] \quad (1)$$

Table 1 Parameters for the Lennard-Jones potential (1).

Interaction	ε(kJ/mol)	σ(nm)
O-O	0.645	0.317
O-Si	1.262	0.327
O-Cl	0.538	0.375
O-Na	0.200	0.286
Cl-Cl	0.445	0.445
Cl-Si	1.044	0.388
Cl-Na	0.166	0.339
Na-Na	0.062	0.257
Na-Si	0.398	0.295

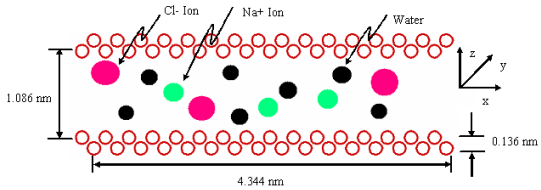

Fig. 1 Schematic of a nano-channel containing water molecules, sodium ions and chloride ions, corresponding to the 3rd kind of fluid treated in this study.

are the same as those for oxygen, see Table 1. Here, r is the distance between ith and jth molecules. We selected this fluid because it will be more convenient in comparatively investigating the effect of the polarization of water (i.e. the second kind of fluid) on the fluid properties. There are 460 molecules in this case.

As the second fluid, the water is modeled by using the SPC/E model, in which the structure is rigid and hydrogen and oxygen are represented by point charges (q_H=+0.425e and q_O=-0.847e). The interaction potential among water molecules is constituted by the Lennard-Jones potential acting between the oxygen-site pairs and the electric potential between all pairs of charged molecules [20]. The number of molecules used in this simulation amounts to 460.

The third fluid is composed of 460 water molecules and 4 pairs of sodium and chloride ions. We enforced the Lennard-Jones potential between oxygen sites of water and ion molecules and the electric potential between charged sites of water and ions [20]. Figure 1 presents an arbitrary distribution of molecules and ions to be subjected to the MD simulation together with the coordinate system.

The channel walls are modeled by two layers of silicon atoms each layer being oriented in the <100> direction [21] (Fig. 1). Typical lateral dimensions of the channels wall are 4.344×4.344 nm which correspond 128 silicon atoms for each layer of channel wall. The walls are separated by 1.086 nm. We considered the interaction between the wall and fluid molecules by using the Lennard-Jones type. The parameters selected for the Lennard-Jones potential (1) are summarized in Table 1.

B. Mathematical models and numerical methods

For each kind of fluids the equations of motions of molecules are different. For the 1st fluid only the translational motion will be considered. For the second and third, rotational motions are additionally considered.

The governing equation for the translational motion of the ith molecule is

$$m_i \frac{d}{dt}\mathbf{v}_i = \mathbf{F}_i , \tag{2}$$

where, m_i is the mass of molecule, $\mathbf{v}_i$ is the velocity and $\mathbf{F}_i$ is the total force exerting on the molecule.

To describe the rotational motion for water molecules, we use the Euler angles combined with the quaternion coordinates [16, 18]. The governing equation for the rotational motion is

$$\frac{d}{dt}\mathbf{I}^s = \boldsymbol{\tau}^s , \tag{3}$$

where, $\mathbf{I}^s$ is the angular momentum and $\boldsymbol{\tau}^s$ is the torque about the center of mass of the molecule in the space-fixed frame.

Next, the angular momentum in body-fixed frame, $\mathbf{I}^b$ is given as

$$\mathbf{I}^b = [A]\,\mathbf{I}^s , \tag{4}$$

where [A] is the rotation matrix defined as

$$[A] = \begin{pmatrix} q_0^2+q_1^2-q_2^2+q_3^2 & 2(q_1q_2+q_0q_3) & 2(q_1q_3-q_0q_2) \\ 2(q_1q_2-q_0q_3) & q_0^2-q_1^2+q_2^2-q_3^2 & 2(q_2q_3+q_0q_1) \\ 2(q_1q_3+q_0q_2) & 2(q_2q_3-q_0q_1) & q_0^2-q_1^2-q_2^2+q_3^2 \end{pmatrix} \tag{5}$$

Here, q_m ($m = 0,1,2,3$) indicates the four components of the quaternion $\mathbf{Q}$ that are related to the Euler angles (φ, θ, ϕ) as follows.

$$\begin{aligned} q_0 &= \cos(\theta/2)\cos\big((\varphi+\phi)/2\big) \\ q_1 &= \sin(\theta/2)\cos\big((\varphi-\phi)/2\big) \\ q_2 &= \sin(\theta/2)\sin\big((\varphi-\phi)/2\big) \\ q_3 &= \cos(\theta/2)\sin\big((\varphi+\phi)/2\big) \end{aligned} \tag{6}$$

Further, we need the dynamical equation for $\mathbf{Q}$ in terms of the angular velocity components defined in the body-fixed frame $(\omega_x^b, \omega_y^b, \omega_z^b)$:

$$\frac{d}{dt}\begin{pmatrix} q_0 \\ q_1 \\ q_2 \\ q_3 \end{pmatrix} = \frac{1}{2}\begin{pmatrix} q_0 & -q_1 & -q_2 & -q_3 \\ q_1 & q_0 & -q_3 & q_2 \\ q_2 & q_3 & q_0 & -q_1 \\ q_3 & -q_2 & q_1 & q_0 \end{pmatrix}\begin{pmatrix} 0 \\ \omega_x^b \\ \omega_y^b \\ \omega_z^b \end{pmatrix} \tag{7}$$

The leap-frog Verlet algorithm was used to integrate these differential equations with the numerical time step ranging from 1.0 to 3.0 fs depending on the type of fluid as well as the density [18].

There are three kinds of forces acting on each molecule including the Lennard-Jones force $\mathbf{f}_{L-J}$, the Coulomb force $\mathbf{f}_C$ and the external force $\mathbf{f}_e$ encompassing the gravitational or electric force. In general, the total force $\mathbf{F}_i$ acting on the ith molecule can be written as:

$$\mathbf{F}_i = \mathbf{f}_{L-J,i} + \mathbf{f}_{C,i} + \mathbf{f}_{e,i} \tag{8}$$

The first term on RHS of Eq. (8) is computed by following formula:

$$\mathbf{f}_{L-J,i} = 24\varepsilon_{ij} \sum_{\mathbf{n}\in Z^2}{}^{*} \sum_j \left[2\left(\frac{\sigma_{ij}}{s_{ij}}\right)^{12} - \left(\frac{\sigma_{ij}}{s_{ij}}\right)^{6} \right] \times \frac{\mathbf{s}_{ij}}{s_{ij}^2} \tag{9}$$

where, $\mathbf{s}_{ij} = \mathbf{r}_{ij} + n_x L_x \mathbf{e}_x + n_y L_y \mathbf{e}_y$, $\mathbf{r}_{ij} = \mathbf{r}_i - \mathbf{r}_j$ and $s_{ij} = |\mathbf{s}_{ij}|$. Further, $\mathbf{e}_x$ and $\mathbf{e}_y$ are unit vectors, $\mathbf{n} = (n_x, n_y)$ a pair of integers, and L_x and L_y denote the spatial size of the physical domain. Here the superscript * indicates the omission of the term with $i = j$ when $\mathbf{n} = 0$. This double summation is effectively computed by applying the minimum-image criterion, cut-off and neighbor algorithm [18-19]. A cutoff

radius of 0.8 nm and a neighbor radius of 1.1 nm are used in this study.

The Coulomb force, i.e. the second term on RHS of Eq. (8), can be obtained from

$$\mathbf{f}_{C,i} = q_i \sum_{\mathbf{n}\in\square^2}{}^{*}\sum_j \frac{q_j}{s_{ij}^2}\frac{\mathbf{s}_{ij}}{s_{ij}} \tag{10}$$

where q_i denotes the charge of the ith molecule. The 3D Ewald-summation can not be directly applied for this double summation, because there is no periodicity in the z-direction, see fig 1. This problem can be overcome by using an equivalent model and adding the correction term [15]. First, we have elongated the simulation domain in the z-direction by adding a vacuum space of 12 nm. With this special treatment, we can apply the periodic boundary conditions for all directions. The effect of such artificial slabs added to the physical slab is insignificant, because the vacuum space is large. Second, we must add correction terms. Thus, Eq. (10) is effectively computed as follows [12, 15].

$$\mathbf{f}_{C,i} = \mathbf{f}_{C,i}^{(r)} + \mathbf{f}_{C,i}^{(k)} + \mathbf{f}_{C,i}^{(c)} \tag{11}$$

Each of the RHS terms are called the real-space, Fourier-space and correction forces, respectively, to be determined by

$$\mathbf{f}_{C,i}^{(r)} = q_i \sum_j q_j \sum_{\mathbf{n}\in Z^3}{}^{*}\left(\frac{2\alpha}{\sqrt{\pi}}\exp\left(-\alpha^2 s_{ij}'^2\right) + \frac{\operatorname{erfc}\left(\alpha s_{ij}'\right)}{s_{ij}'}\right)\frac{\mathbf{s}_{ij}'}{s_{ij}'^2} \tag{12}$$

$$\mathbf{f}_{C,i}^{(k)} = \frac{q_i}{V}\sum_j q_j \sum_{\mathbf{k}\neq 0}\frac{4\pi\mathbf{k}}{k^2}\exp\left(-\frac{k^2}{4\alpha^2}\right)\sin\left(\mathbf{k}\cdot\mathbf{r}_{ij}\right) \tag{13}$$

$$\mathbf{f}_{C,i}^{(c)} = \left(-\frac{4\pi q_i}{V}\sum_j q_j z_j\right)\mathbf{e}_z \tag{14}$$

where, $\mathbf{s}_{ij}' = \mathbf{r}_{ij} + n_x L_x \mathbf{e}_x + n_y L_y \mathbf{e}_y + n_z L_{z,new}\mathbf{e}_z$, $s_{ij}' = \left|\mathbf{s}_{ij}'\right|$, $V = L_x L_y L_{z,new}$, α is the splitting parameter of the Ewald sum having the dimension of inverse of length, which controls the relative importance of contributions coming from the real and reciprocal space (Fourier space), and the vector $\mathbf{k}$ is the discrete set $\left(2\pi/L_x, 2\pi/L_y, 2\pi/L_{z,new}\right)Z^3$.

The first term on the RHS of Eq. (11) rapidly falls to zero with the distance s_{ij}', so we selected a cutoff radius of 1.1 nm and a neighbor radius of 1.4 nm. The second term was effectively computed by applying the PPPM method (Particle-Particle-Particle-Mesh) [13, 14]. In this method, an FFT grid spacing of 0.12nm and a TSC (triangular shaped cloud, 2nd order) for the charge distribution and the force interpolation were chosen. We assume that the performance of the charge assignment and the force interpolation can be improved by using the minimum-image criterion, the cut-off and neighbor list methods. The third term of Eq. (11) contributes to Coulomb force from the z-component of the total dipole moment of the simulation slab [15].

The last term of Eq. (8) is the external force which is considered only for the non-equilibrium molecular-dynamic simulations. In this study, we considered only the gravity force.

To avoid the viscous heating, the Berendsen thermostat was used with the time constant 0.1 ps [7, 18]. Then velocities were rescaled as follows.

$$\mathbf{v}_{\text{new}} = \chi \mathbf{v}_{\text{old}} \tag{15}$$

where the rescaling parameter χ reads

$$\chi = \left[1 - \frac{\Delta t}{\tau}\left(\frac{T_{\text{desire}}}{T} - 1\right)\right]^{1/2} \tag{16}$$

Here T_{desire} is a desired temperature, i.e. 300K and T is the temperature at (t-Δt/2) to be calculated from the general formula for the rigid molecule:

$$fNk_{\text{B}}T = \sum_{i=1}^{N}\left[m_i v_i^2 + \boldsymbol{\omega}_i^b \cdot \mathbf{I}\cdot\boldsymbol{\omega}_i^b\right] \tag{17}$$

where, $\mathbf{I}$ is the moment of inertia tensor, f is the number of degree of freedom (e. g, six for the water molecules and three for other molecules), k_B is the Boltzmann's constant, N is the number of molecules. The temperature T was calculated self consistently with three iterations. In non-equilibrium molecular-dynamic simulation, there is non-trivial streaming flow along the channel, so the motion of molecules is constituted from two types; one is the streaming motion and the other the thermal motion. However, the streaming velocity is so small compared to the velocity by the thermal motion. Hence, we neglected the influence of the streaming velocity in determining the thermal kinetic energy.

Before starting the MD simulation, the initial positions, orientation, translational and rotational velocities of all the molecules have to be assigned. The velocities were chosen randomly from a Gaussian distribution with magnitudes that should contribute to the half of the set-up temperature 300K, after which they are corrected so that no overall linear momentum is produced. We set up the rotational velocities for each water molecule in a similar way. We set the values randomly but contributing again to the half of the temperature at 300K, being corrected so that there is no overall angular momentum [18].

We used the Euler angles combined with quaternion coordinates to describe the motion of rigid water molecules, so we must pay attention to setting the initial positions and orientations of molecules such that the intermolecular force and the torque should not be so large. By using the energy minimization [6, 8], we could set up a configuration that reveals reasonably small interaction forces. However, even for small forces, the system may independently show large interaction torques. So we proposed a plausible algorithm to avoid large torque. Firstly, all molecules were assigned with random positions and orientations. While keeping the orientations of the water molecules we performed the energy minimization to find the initial positions having small forces. The steepest descent method combined with the conjugate gradient method was applied in this energy minimization. To implement the line minimization, we used the Brent method and parabolic interpolation [17] with the spatial step size for the line search 0.01nm. After this first step, we can get a configuration with small interaction force, but the interaction moment can be large. In order to reduce the torque we add damping terms to Eqs. (2) and (3). Then, the equations of motions become

$$m_i \frac{d}{dt}\mathbf{v}_i = \mathbf{F}_i - \alpha_F \mathbf{v}_i \tag{18}$$

$$\frac{d}{dt}\mathbf{I}^s = \boldsymbol{\tau}^s - \alpha_T \mathbf{I}^s \tag{19}$$

where α_F and α_T are the damping coefficients for the force and the moment, respectively. In our study, we chose α_F =0.732 N·ps/m and α_T =12.8 J·ps/mol. We set zero as the initial values for integration of Eqs. (18) and (19). The above processes were performed in a subspace (i.e. a quarter space in the (x,y) plane) following the idea of [7]. After that, we copied the set-up obtained in this way to all the other subspaces for use as the initial conditions for the MD simulation.

In the non-equilibrium molecular-dynamic simulation, we applied the gravity force in the x-direction. The gravity force acting on a molecule varied from 68 to 406 fN (typically a factor of 10^8). The reason for application of such high gravity force is that since the interactive force between molecules themselves and that between the wall and molecules is so large that the statistical error becomes so high if the actual gravity force were applied.

To reach the steady state, the system was simulated for the time duration 0.4-0.8 ns. After the system reached the steady state, we performed sampling every 10 time steps in order to compute the average statistics for 0.3-1 ns except for the velocity autocorrelation functions (VACF) and the diffusion coefficients. For the VACF, the sampling was performed every 10 time steps for 0.05 ns. The binning method was used to compute the density and velocity profile across the channel.

3. RESULTS AND DISCUSSION

As the first step, the equilibrium MD simulation has been performed. We present the numerical results of the density profile, the radial distribution function and the velocity autocorrelation function obtained in this simulation.

A. Density profiles

The number density is defined as:

$$\rho(n) = \frac{1}{A\Delta z M}\sum_{j=1}^{M}\sum_{i=1}^{N} H_n\left(z_{i,j}\right) \tag{20}$$

$$H_n\left(z_{i,j}\right) = 1 \quad \text{if} \quad (n-1)\Delta z \prec z_{i,j} \prec n\Delta z \tag{21}$$

where M is the numbers of samples and N is the number of particles. The attractive interaction between the wall and the fluid molecules result in the space adjacent to wall that is devoid of the fluid molecules. So, an effective distance L_z' normal to the wall accessible to the fluid molecules was quantified as

$$L_z' = L_z - 2\delta \tag{22}$$

where, δ is a gap of the space adjacent to wall. In this paper, we evaluated the gap δ equal to 0.16, 0.3 and 0.3 nm for the Lennard-Jones fluid, the water fluid and the aqueous sodium-chloride solution cases, respectively [3]. This leads to the effective number density

$$\rho_{eff} = \frac{N}{L_x L_y L_z'} \tag{23}$$

z-direction in the channel. In (a), the green, black and pink colors indicate water, solution and Lennard-Jones fluid, respectively. In (b), the blue and pink colors indicate the chloride and sodium ions, respectively.

The number density profiles of the Lennard-Jones molecules, the center of mass of the water molecules, sodium ions as well as chloride ions are shown in Fig. 2. All the

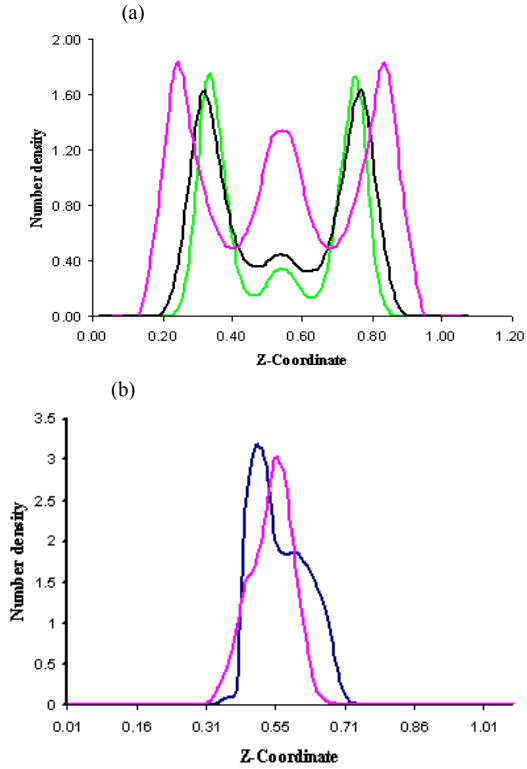

Fig. 2 The number density profile of each molecule along

number densities were normalized with their effective number densities. Figure 2(a) shows three maximum peaks with one lower peak in mid-channel indicating three-layer structure in the channel. The two layers adjacent to walls are formed by the fluid-wall interaction. This can be understood by estimating the Lennard-Jones potential between fluid molecules and the wall as shown in Fig. 3. These layers affect molecules in the mid of the channel and show high density (in particular for Lennard-Jones fluid). It is clear that the direct effect of walls on those molecules is weak.

Hence, the formation of layers in the mid-channel is mainly due to the layers adjacent to the wall. We see that the peak in the mid-channel is so lower than the other peaks for the water fluid and aqueous sodium-chloride solution cases and the high peaks in the Lennard-Jones fluid case is closer to wall than those of the other cases. This is due to the influence of the electric force on the motion of molecules. Further, Fig. 2(a) shows that the number density profiles in the water fluid and aqueous sodium-chloride solution cases are not largely different from each other. This implies that the effect of the presence of ions on this property is not considerable. Figure 2(b) shows the number density profile for the sodium and chloride ions. We see that those ions only concentrate in the mid-channel because of the formation of two water layers close to wall.

B. Radial distribution function

In the previous section, we considered the density distribution in z-direction. From this result, we can get some information about the structure of liquid in the channel, but that is only in the z-direction. To understand further about it in the x-y plane, we computed the radial distribution function in the x-y plane that was defined as

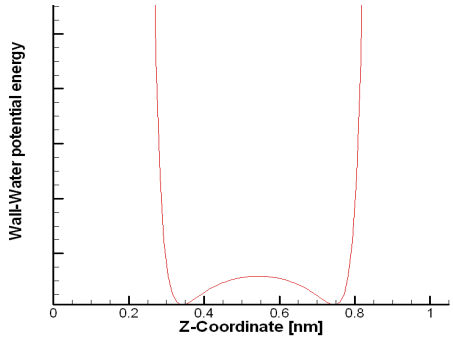

Fig. 3 The Lennard-Jones potential of the wall-water interaction as a function of the position (z-coordinate) of the water molecule

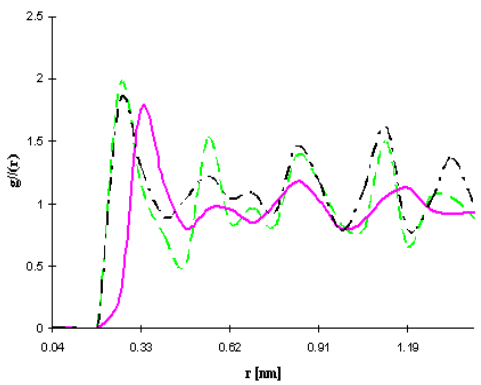

Fig. 4 The lateral radial distribution function g//(r) in the plane parallel to the wall; green - water, black - solution and pink - Lennard-Jones

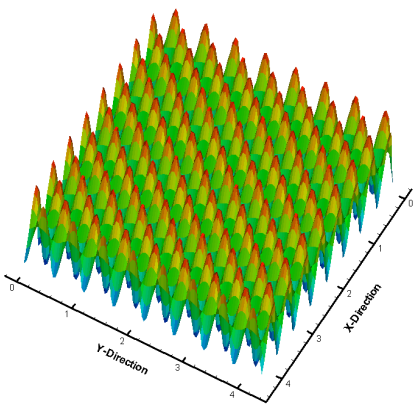

Fig. 5 The Lennard-Jones potential of the wall-water interaction in the x-y plane

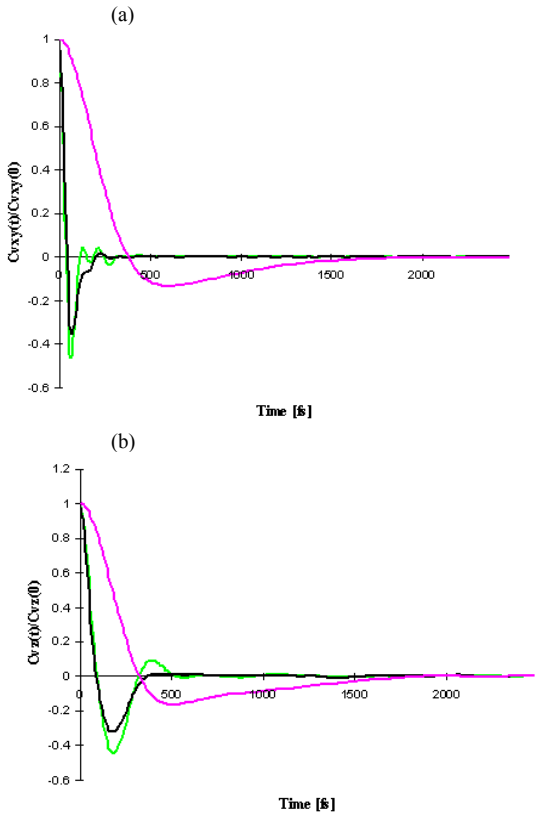

Fig. 6 The Velocity autocorrelation functions of the fluid molecules; green - water, black – solution, pink - Lennard-Jones. We normalized them by the value at t = 0

$$g_{//}(r)=\frac{1}{\rho^2 V}\sum_{i\neq j}\delta\left(r-r_{ij}\right)\left[\theta\left(\left|z_i-z_j\right|-\frac{\delta z}{2}\right)-\theta\left(\left|z_i-z_j\right|+\frac{\delta z}{2}\right)\right] \quad (24)$$

where V is the volume, r_{ij} is distance parallel to the x-y plane between molecules i and j, z_i is the z coordinate and δ(x) is the Dirac delta function. The Heaviside function θ(x) restricts the sum to a pair molecules located in the same slab of width δz. The physical interpretation of $g_{//}(r)$ is that $g_{//}2\pi r dr\delta z$ is proportional to the probability of finding a molecule in a slab of thickness δz at a distance r parallel to the walls from a randomly chosen molecule. In a bulk liquid, this would be identical to g(r), the standard RDF.

Figure 4 shows the radial distribution function of the center of molecular mass of different fluids. The approximated long-range order indicates that the system has adopted the approximated crystalline phase. This can be explained by considering the Lennerd-Jones potential between the fluid molecules and the wall (Fig. 5). We see that a distance between two long-rage adjacent peaks in Fig. 4 is approximately equal to those in Fig. 5. This implies that the approximated crystalline phase is due to wall. The difference of the radial distribution function for different fluids indicates that the electric force as well as the presence of ions in solution strongly affects this property of fluid.

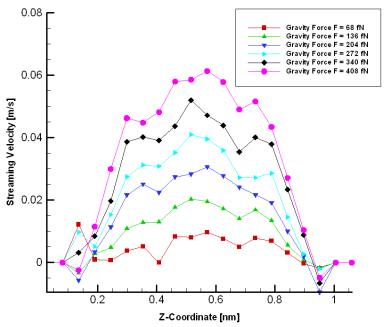

Fig. 7 The streaming velocity in the x-direction for different values of the gravity force

C. Velocity autocorrelation function

We computed the velocity autocorrelation function and diffusion of molecules to consider the diffusivity in the dynamic property of the fluid confined in a slit channel. The autocorrelation function of a quantity X can be defined as

$$c_X(t) = \langle X(t)X(0)\rangle = \frac{1}{MN}\sum_{j=1}^{M}\sum_{i=1}^{N} X_i(t_j)X_i(t_j+t) \qquad (25)$$

where M is the number of time origins and N is the number of molecules in the system. If the quantity X is velocity then autocorrelation function is the so-called velocity autocorrelation function (VACF).

Figure 6 shows the z-direction VACF and the x-y plane VACF of fluid molecules in the channel. We normalized the VACF by the value at t=0. Both the z-direction and x-y plane VACF of molecules in the water fluid and the aqueous sodium-chloride solution cases initially rapidly decrease and then increase again compared to those in the Lennard-Jones fluid case. And the minimum VACF of Lennar-Jones molecules are higher than those of other molecules. This can be explained by considering the number density; that is, for a higher number density we expect a more fluctuation of VACF [19]. As seen in the previous section, we see that the effective number densities for both electrolyte fluids, i.e., the water fluid and the aqueous sodium-chloride solution, are larger than that in Lennard-Jones fluid. Further, the VACF of molecules in both the water fluid and the aqueous sodium-chloride solution approximately reach the minimum as well as maximum values at the same time. These indicate that the VACF of molecules are strongly affected by the electric force, and with dilute solution the effect of the presence of ions on this property is weak.

D. The velocity profile and the flow rate

The non-equilibrium molecular-dynamic simulation was performed, in the second step, by applying a uniform gravity force parallel to the wall for each molecule. This case is similar to the case where the flow is created by applying a pressure gradient along the channel. In our study, the gravity force is related to the pressure gradient as follows.

$$F_{gravity} = \frac{\partial P}{\partial x} L_x (L_y L_z)\frac{1}{N} \qquad (26)$$

To study the flow property in the nano-channel, we considered the velocity profile that can be obtained from

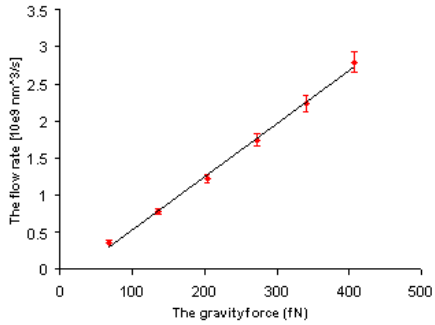

FIG. 8. Flow rate versus the gravity force with a 95% confidence

$$v(z_n) = \frac{1}{M}\sum_{j=1}^{M}\frac{\sum_{i=1}^{N} H_n(z_{i,j})v_{i,j}^x}{\sum_{i=1}^{N} H_n(z_{i,j})} \qquad (27)$$

where, $z_n = \left(n-\frac{1}{2}\right)\Delta z$ and $H_n(z_{i,j})$ was given in Eq. (21).

Figure 7 shows the velocity profile for different gravity forces. Unexpectedly the velocity profiles are not parabolic; there are ranges respond to those of valleys in the number density profile in where the streaming velocity has characteristics different to other range. This was clearly explained by Travis et al [1]. The velocity close to wall is negative because of the statistical noise.

Next we calculated the flow rate, defined as

$$Q_x = \int_{z_{lower}}^{z_{upper}} v_x(z)dz \qquad (28)$$

Figure 8 shows the flow rate varied with the gravity force. It is seen that the flow rate is linearly varied with the gravity force with a 95% confidence. This is consistent with the classical theory for fully-developed fluid flow through a channel.

4. CONCLUSION

We developed the FORTRANS code to perform MD simulation by using the Euler angles for the constraint of rigid molecules. The disadvantage of using the Euler angles in MD simulation have been overcome by adding the damping force and the damping moment in setting up the initial configuration.

For the number density profile, the electric force strongly affects this property in the small channel, (in particularly, the gap is appro 3 times diameter of molecules). And this property is not considerably changed by the presence of ions in the solution that is not so dense. With the small channel, the property of fluid is strongly dependent to the characteristic of the wall. We considered the radial distribution function and found that the fluid has adopted the approximated crystalline phase by the influence of wall. These indicate that the equilibrium properties of fluid in the small channel are strongly influenced by the electric force as well as the characteristic of the wall.

From non-equilibrium MD simulations, we found that the dynamical properties are strongly affected by both the electric

force and the characteristic of the wall. Thus, we have to consider the electric force in MD simulation for water molecules confined in a small channel. We have also obtained the streaming velocity profile and the flow rate in the channel for different gravity forces. The velocity profiles are not parabolic; this result is similar to that observed by Travis et al [1]. The flow rate is linearly dependent on the gravity force; this behavior is similar to that observed in the macro-channel.

ACKNOWLEDGMENTS

This work was supported by the Korea Science and Enginee-ring Foundation (KOSEF) through the National Research Labo-ratory Program funded by the Ministry of Science and Technol-ogy (No. 2005-1091)

REFERENCES

[1] Travis, K. P. and Gubbins, K. E., J. Chem. Phys. 112, 1984 (2000)
[2] Xu, J. L and Zhou, Z. Q, Heat and Mass Transfer. 40 859-869 (2004)
[3] Kumar, P., Buldyrev, S. V., Starr, F. W., Giovambattista. N. and Stanley, H. E., Phys. Rev. E. 72, 051503 (2005)
[4] Kumar, P., Starr, F. W., Buldyrev, S. V., and Stanley, H. E., Phys. Rev. E. 75, 011202 (2007)
[5] Zangi. R. and Mark, A. E., J. Chem. Phys. 119, 1694 (2003)
[6] Qiao, R. and Alura, N. R., J. Chem. Phys. 118, 4692 (2002)
[7] Freund, J. B., J. Chem. Phys. 116, 2194 (2002)
[8] Kim, D. and Darve, E., Phys. Rev. E. 73, 051203 (2006)
[9] Wang, M. and Chen. S., Common. Comptu. Phys. 3, 1087-1099 (2008)
[10] Kim, C. S., ASME 129, 1140 (2007)
[11] Atamas, A. A., Atamas, N. A. and Bulavin, L. A., J. Mol. Liq. 120, 15-17 (2005)
[12] Brodka, A., J. Mol. Struc. 792-793, 56-61 (2006)
[13] Deserno, M. and Holm, C., J. Chem. Phys. 109, 7678 (1998)
[14] Deserno, M. and Holm, C., J. Chem. Phys. 109, 7694 (1998)
[15] In-Chul Yeh and Max L. Berkowitz, J. Chem. Phys. 111, 3155 (1999)
[16] Hiyama, M., Kinjo, T. and Hyodo, S. A., J. Phys. Soc. Japan. 77, 064001 (2008)
[17] Press, W. H., Teukolsky, S. A., Vetterling, W. T. and Flannery, B. P., Numerical recipes in the Fortrans 77, Publisher Press Syndicate (1992)
[18] Allen, M. P. and Tildesley, D. J., Computer Simulation of Liquids, Publisher Press Inc., New York (1987)
[19] Haile, J. M., Molecular Dynamcis Simulation, Publisher Wiley-interscience (1997)
[20] Rapaport. D. C., The art of Molecular Dynamics Simulations, Publisher Press Syndicate (1995)
[21] http://en.wikipedia.org/wiki/silicon